

**SMASIS2022-90377**

**METHODS FOR THE RAPID DETECTION OF BOUNDARY CONDITION VARIATIONS IN  
STRUCTURAL SYSTEMS**

**Xuyang Li**  
Michigan State University  
East Lansing, MI

**Talal Salem**  
Michigan State University  
East Lansing, MI

**Hamed Bolandi**  
Michigan State University  
East Lansing, MI

**Vishnu Boddeti**  
Michigan State University  
East Lansing, MI

**Nizar Lajnef**  
Michigan State University  
East Lansing, MI

**ABSTRACT**

*This study proposes a novel anomaly detection approach focusing on structural components which do not have a baseline model and with complex boundary conditions that cannot be built into a finite element or a digital twin model. The approach uses only sensor collected compressed response distribution data to detect and localize changes in boundary conditions under extreme loading events. The developed methods use unsupervised anomaly detection networks combined with novel data compression algorithms. The deep network collects training data from real direct measured responses of the structural system over time to build a model and then computes the reconstruction errors and identifies anomalies. A simplified gusset plate under variable clamped-clamped boundary conditions is used in this study as preliminary proof-of-concept. In this work, anomalies are induced by changing the connection conditions (boundary conditions) of the gusset plate (e.g. bolts loosening). This study improved the deep learning network performance by incorporating mechanics-based loss functions into the network, fed with experimental data obtained from the distributed sensors installed on the structural element. Results show that the mechanics-based modified loss function significantly improves the identification and localization abilities of boundary condition anomalies and eliminates undesired factors and false predictions.*

Keywords: damage detection and localization, machine learning, gusset plates, structural health monitoring

**1. INTRODUCTION**

One of main challenges in applying Structural Health Monitoring (SHM) methods has been always the lack of accurate models for existing structural systems. Establishing a baseline model for most systems is either impractical or infeasible due to the non-existence of design and construction or design information. Even though SHM has been widely applied to bridges [1, 2], skyscrapers [3, 4], wind turbines [5, 6], data handling and processing remains largely ineffective for real large-scale systems under field loading conditions. Typically, the tremendous amount of collected data needs to be denoised, missing data needs to be restored, and the information processed to obtain useful actionable results. Many studies proposed different approaches to successfully overcome these obstacles using machine learning [7-10], Bayesian models [9, 11], and other data fusion methods [2, 9], but the amount unusable data remain a major problem. Moreover, it is worth noting that recently, machine learning is increasingly applied in structural damage detection and structural condition assessment of civil infrastructures with various degrees of success. Several studies showed that using machine learning tends in general to improve the performance in term of speed and accuracy compared with the existing SHM tools [12-14]. One of the many issues that have generally hampered the use of advanced ML methods in civil engineering applications is the quality of data and in some cases the forced adaption of inadequate data to methods directly borrowed from other fields. In this preliminary work, we intend to show the advantages of an efficient data handling approach (reduction in this case) combined with an ML method.

Convolutional neural networks (CNNs) are one of the most heavily applied techniques. For example, a residual CNN was

proposed for structural modal identification using de-noised signals in [15]. CNNs were also used for real-time monitoring and vibration-based structural condition assessment [16-18]. Besides feed-forward neural networks, it is worth mentioning that several sequence-based models were also employed to detect, localize, and quantify the structural defects. On the other hand, long short-term memory (LSTM) (i.e., an advanced type of recurrent neural network - RNN) was investigated for damage detection in wind turbine blades [19], rubber bearing [20], and offshore structures [21]. Furthermore, autoencoders were used with a reconstruction model of structural responses to detect concrete cracks in collected images [22-25]. In [26], compressive sensing was developed and the reconstructed responses were used for structural damage detection and localization. Furthermore, special types of machine learning models such as zero-shots and few-shots learning and detection are widely used to recognize and disjoin training classes and unseen classes or anomalies [27-32], where no anomaly or few anomaly data are used for model training. In our work, we are focusing on the latter techniques.

In this work, the ML approaches are augmented, as stated above, with experimental sensing data to establish baseline raining. Among the existing SHM sensing technologies, strain gauges are commonly used to components' condition [33]. Strain gauges offer several advantages such as high reliability and flexibility (shape and size) and the low cost associated with their manufacturing process [34-38]. For instance, strain gauges were used for damage identification in plate structures [39], bridges [39-41], concrete structures [42], and highway sections [43, 44]. However, strain gauge measurements may provide misleading information due to the overlap between strain events (i.e., resulting from structural damages or environmental factors) [45]. To address such issues, the structure can be monitored continuously and data is recorded for whole loading events. For example, strain data measured from a long-span suspension bridge were compressed and recovered using an autoencoder network for data anomaly detection [46]. Several data compression algorithms were developed to reduce data size and data latency [45-48]. Recently, self-powered floating gate sensors powered by strain energy were used in wireless sensor networks to detect, localize and quantify damage [49-51].

This paper presents a new approach for detecting and localizing structural damage with unsupervised deep learning. Our approach does not involve any labeling or damaged instances during model training. Only data from the undamaged intact structures were used. The reconstruction error was set to serve as a metric to assess the abnormality in the data and determine the source of the data (e.g., undamaged or damaged instances) [50]. The unique features of the reported approach can be summarized as (i) a combination of variational autoencoder neural network and LSTM network using highly compressed SHM data is used, which can detect and localize structural damages, (ii) an unsupervised neural network is trained without foreseeing anomalies or any damage instance, (iii) a new physics-informed network loss function based on the spatial information is presented to improve the damage detection and

localization abilities, and (iv) efficient and fast (only requires a short time to gather few samples for neural network testing). The paper is organized as follows. Section 2 presents a short summary background of deep learning, and schematic strategy for the data reduction method and anomaly detection approaches. Sections 3 and 4 show the use of the proposed unsupervised deep neural network for anomaly detection and localization through experimental results. The network is retrained using a custom loss function based on basic mechanical characteristics to further improve the model performance. Section 5 summarizes the major findings of the study.

## 2. FRAMEWORK OF DEEP LEARNING-BASED DATA ANOMALY DETECTION

### 2.1 Background of anomaly detection

Anomaly detection refers to a detection technique for finding patterns or instances that do not resemble the data with expected behaviors [51, 52]. Such dissimilarity in properties might be hard to find but can be isolated with relevant data processing. Anomaly detection has been used in the field of malware [53, 54], financial fraud detection [55, 56], and SHM [57, 58]. Many methods are used including isolation forest [59], graph-based anomaly detection [55], entropy-based networks [53], discriminative metric learning [60], and deep anomaly detection networks [51].

In structural damage detection applications, differences in structural properties between undamaged and damaged structures can be discovered and used to differentiate the structural status using computer vision [58], generative adversarial networks (GANs) [61], autoencoders, or reconstruction-based models [25, 61]. Specifically, in reconstruction-based models, many approaches use reconstruction discrepancies from sensor data obtained from two different states of structures [46, 62, 63]. By adding a Gaussian anomaly prior to assumption, variational autoencoders are also used for SHM [64, 65].

### 2.2 Implemented data reduction technique

In this work we adopt a data reduction approach based on the extraction of data distribution features from continuous sensing data streams. Instead of feeding whole strain vs time data streams into the network, the time history output is analyzed to derive distribution characteristics [49, 66]. First, different thresholds are selected based on the strain event responses. Then the duration of strain events higher than a threshold is recorded and added up to get cumulative time data (i.e., each threshold results in one cumulative time data). The cumulative time results in Gaussian cumulative density functions (CDFs) represented by Eq. (1), and the Gaussian parameters can be obtained by curve fitting as shown in Fig. 2 (b).

$$F_{Gaussian}(\varepsilon) = \frac{\alpha}{2} \left[ 1 - \operatorname{erf} \left( \frac{\varepsilon - \mu}{\sigma\sqrt{2}} \right) \right] \quad (1)$$

$\alpha$  is the summation of all cumulative time events,  $\mu$  and  $\sigma$  represent the mean and standard deviation of the cumulative density function, erf denotes the Gauss error function.

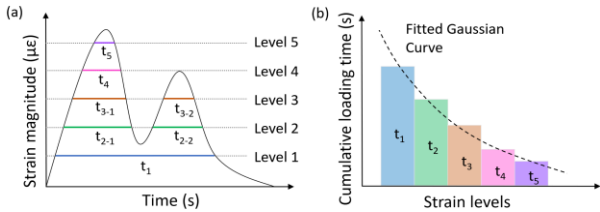


**FIGURE 1:** Representation of the data reduction approach (a) strain response and preset strain levels; (b) curve fitting of cumulative loading time.

The characteristic of  $\mu$  and  $\sigma$  obtained from curve fitting can be used for structure damage indication. Specifically, different parameters  $\mu$  and  $\sigma$  calculated from different periods of strain events can be plotted as different probability distributions functions (PDF), and the damage occurrence or propagation can be seen visually as the PDF shifts [68]. However, such a one-to-one comparison of different strain events can only assess local damage conditions and is easily disturbed by abnormal or extreme events.

The proposed method takes a sequential data that consists of many pairs of  $\mu$  and  $\sigma$  from a continuous strain output signal, each pair of  $\mu$  and  $\sigma$  is calculated based on one sliced strain response segment which extracted from the full strain event as shown in Fig. 2. These sequential data are further processed in the deep anomaly detection network.

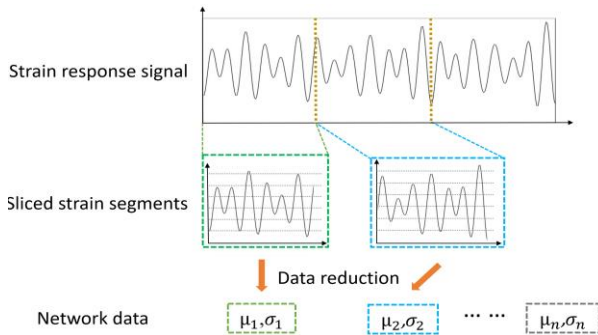


**FIGURE 2:** Framework of data collection and data pre-processing.

### 2.3 Unsupervised deep anomaly detection

The schematic diagram of the unsupervised deep anomaly detection method is shown in Fig. 3. Service level loads are applied to an undamaged structure to generate strain responses and network training data (which are the sequence of  $\mu$  and  $\sigma$ ). The network is then trained, and the undamaged structure baseline is established through the reconstruction of the validation dataset. For damage identification, the testing dataset obtained from the damaged structure and the reconstruction from the testing dataset is compared with the baseline. Furthermore, a

mechanics-based loss function is employed and the network is retrained for better damage localization.

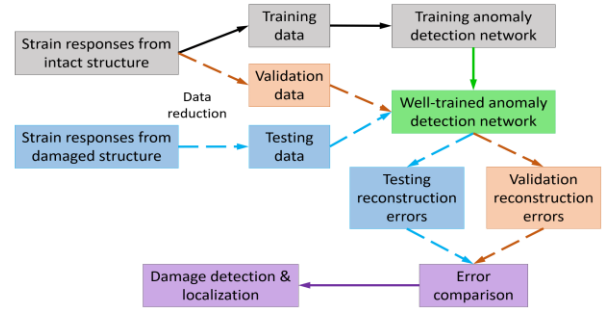


**FIGURE 3:** Schematic diagram of the proposed unsupervised deep anomaly detection network.

## 3. DAMAGE DETECTION AND LOCALIZATION OF GUSSET PLATES

Structural components connected using gusset plates largely depend on bolted connections. It is vital that bolt damage at bridge joints is detected early before any critical failure. This section uses the proposed data processing method and deep anomaly detection neural network for detecting the occurrence of bolt loosening and the localization of the damaged bolt area.

### 3.1 Experiment setup and Data generation

In this study, a steel plate (45 cm x 36 cm) was used for lab testing as shown in Fig. 4. The plate is clamped on the top and bottom sides. The top is fixed and the bottom side is loaded with random forces controlled by an MTS loading frame in a displacement-control configuration. The force is applied with a timestep of 0.1s and all the strain data were recorded with a sampling rate of 1kHz. A total of 27 strain sensors (i.e., strain gauge type is 1-LY11-6/350 measuring the strain in the y-direction) were attached to the plate for data collection as shown in Fig. 4(b). The plate was loaded for only 3 hours, which is sufficient for a baseline model to be built. After the first loading experiment, the bottom bolt was loosened manually and loaded with a random signal of the same duration.

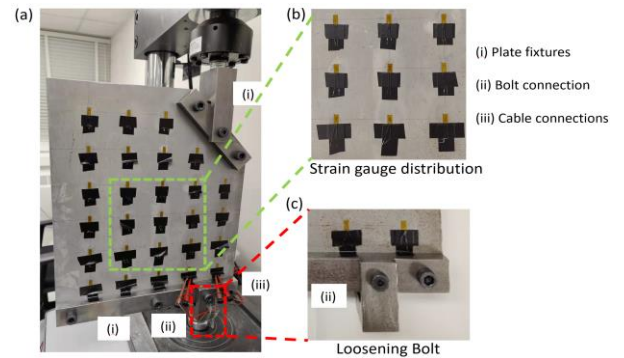


**FIGURE 4:** Experimental setup.

The data reduction method was then used to process both the baseline and anomaly strain responses. Fixed length signal

interval windows were used to calculate the Gaussian parameters with the preset strain threshold levels from Table 1. The obtained parameters are grouped as a dataset input for the neural network.

**TABLE 1:** Preselected strain levels.

Level Number	Strain Threshold Level ( $\mu\epsilon$ )
1	20
2	37
3	54
4	71
5	88
6	105
7	122

### 3.2 Anomaly detection network training

The network uses two-dimensional data input and the output is a reconstruction of the input. The data is arranged in subsets of 12 rows representing the 12 continuous observations and 54 columns representing the 54 parameters obtained from the 27 sensors (i.e., each sensor has two parameters  $\mu$  and  $\sigma$ ). The network consists of an encoder, decoder, LSTM layers, and random variances as shown in Fig. 5.

For the conducted test, the total number of samples is 369 and the training ratio is 0.75. The model is trained for 150 epochs with Adam optimizer and the learning rate is  $5e-5$ . The same number of data samples was obtained from testing the bolt damaged condition, and then fed into the pre-trained network for anomaly detection.

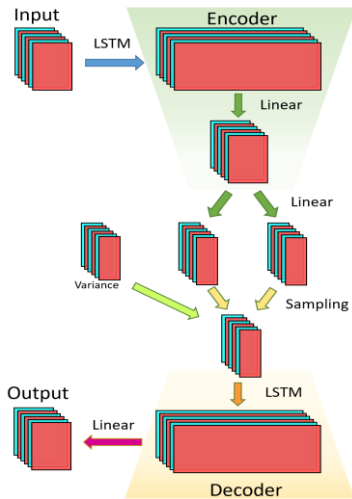


**FIGURE 5:** Proposed network architecture.

The loss function of the network was calculated as the summation of mean square error (MSE) and the KL divergence term (i.e., a strong prior for latent variable values) using the following equations.

$$loss_{MSE} = \frac{1}{n} \sum (\mathbf{y} - \mathbf{x})^2 \quad (2)$$

$$loss_{KL} = -0.5 * \frac{1}{n} \sum (1 + \log(var) - mean^2 - var) \quad (3)$$

$$loss = loss_{MSE} + loss_{KL} \quad (4)$$

Where  $n$ ,  $x$  and  $y$  denote the number of samples, the input and the output from the anomaly detection network. Respectively,  $mean$  and  $var$  are the mean and variance of the latent distribution generated by the encoder network. The training and validation losses are shown in Fig. 6.

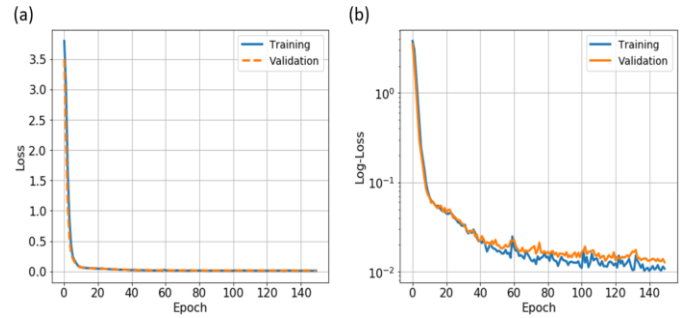


**FIGURE 6:** Training and validation losses with two scales (a) linear scale; (b) logarithmic scale.

## 4. RESULTS AND DISCUSSION

### 4.1 Damage detection results

From the network output, or the reconstruction of the input, each sensor parameter corresponds to a vector of 12 rows. The reconstruction error based on each sensor (or parameter) between the input and output can be calculated using Eq. (5) below.

$$error_j = \frac{1}{12} \sum_{i=1}^{12} (y_{ij} - x_{ij})^2 \quad (5)$$

Where  $error_j$ , 12,  $x$  and  $y$  refer to the  $j^{th}$  parameters for one of the sensors, 12 observations in the time sequence, the input and output of the network, respectively.

For the baseline model where the bolt is fully tightened and the plate is fixed, the sensor reconstruction errors from the training dataset and the validation dataset should be very close in values because of the homology of these two datasets. Considering hundreds of training and validation samples were used, the distributions of those errors were plotted in histograms. Two of the 90 histograms are shown in Fig. 7. The distribution of the two sets of errors is matched, which validates the homology of training and validation datasets and there are no anomalies detected.

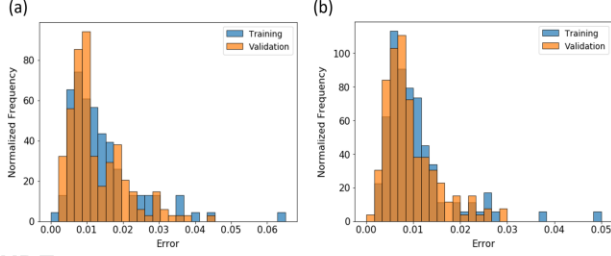


**FIGURE 7:** Loss histograms of training and validation datasets (a) sensor 3 parameter  $\sigma$ ; (b) sensor 2 parameter  $\mu$ .

Compared to the baseline model, the testing dataset from the bolt loosening scenario was fed into the trained network and the errors were compared with the errors from the validation dataset. Sample histograms are shown below in Fig. 8 indicating that the bolt damaged case has higher reconstruction errors than the baseline model and thus, the existence of anomalies.

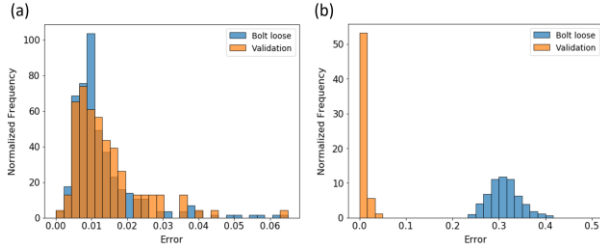


**FIGURE 8:** Loss histograms of damaged sample (a) sensor 3 parameter  $\sigma$ ; (b) sensor 2 parameter  $\mu$ .

To further assess the anomaly detection performance, we employed a binary classification algorithm called receiver operating characteristic (ROC). A vertical cut-off line can be moved from the minimum value to the maximum value of the whole dataset to differentiate the two datasets. Accordingly, the true positive rates and false-positive rates can be calculated for each cut-off value and the calculated data can be plotted as the ROC curve as represented in Fig. 9. Besides, the area under the receiver operating characteristic (AUROC) can also be computed for all 27 sensors to judge the anomaly detection quantitatively. The 27 AUROC values can be plotted as a contour based on the sensors' locations for a better visualization (i.e., Anomalies can be easily found by looking at the color differences). The AUROC contours for the baseline model and the bolt damaged model are plotted in Fig. 10. The yellow background is the plate geometry and the black dots are the sensors (i.e., 'S1' means sensor number 1). For the baseline model, the AUROC values for both parameters  $\mu$  and  $\sigma$  are close to 0.5, which means the training dataset and validation dataset are hard to differentiate. For the bolt damaged model, the values vary for different sensors, but the overall contour displays a huge contrast with blue and red colors, where values are close to the lower and upper limits (i.e., 0 and 1). Such results demonstrate the occurrence of anomalies, which in this case, is the loosened bolt of the plate.

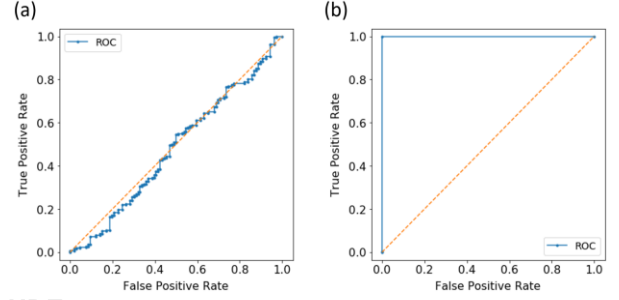


**FIGURE 9:** ROC curve (a) sensor 3 parameter  $\sigma$ ; (b) sensor 2 parameter  $\mu$ .

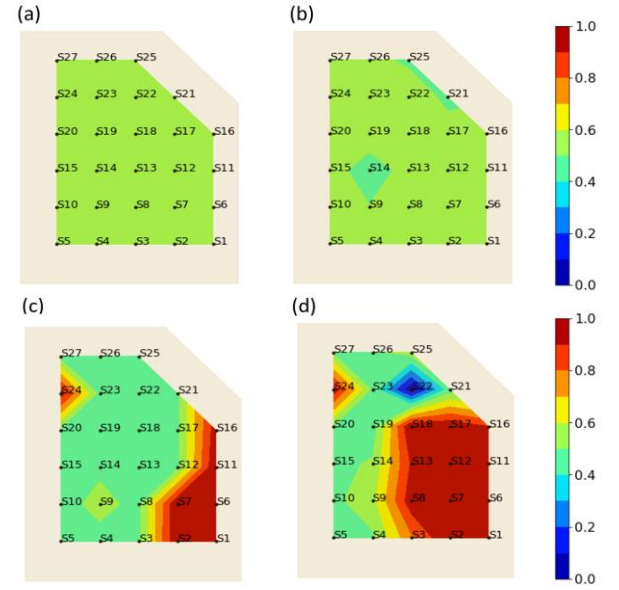


**FIGURE 10:** AUROC contours (a) parameter  $\mu$  in undamaged plate; (b) parameter  $\sigma$  in undamaged plate; (c) parameter  $\mu$  in bolt damaged plate; (d) parameter  $\sigma$  in bolt damaged plate.

## 4.2 Damage localization results

AUROC contours allow for anomaly (damage) detection, however it is hard to accurately localize the anomaly locations (boundary condition or other damage types). Such binary classification method performs well in detection but not localization. An approach that modifies the error for anomaly localization is introduced,

$$Error^* = \frac{|error_{val} - error_{test}|}{Norm(x_{val})} \quad (6)$$

Where  $error_{val}$  and  $error_{test}$  represent the reconstruction errors obtained from the validation or testing dataset and can be obtained using Eq. (5), while  $Norm(x_{val})$  refers to the norm vector on the time sequence dimension of the validation input data  $x_{val}$ .

The 27 modified error values can also be plotted as a contour based on the sensor location information. The baseline model was also evaluated by comparing the training dataset to the

validation dataset. The contours for the baseline model and the anomaly case are displayed in Fig. 11. Fig. 11 (a) and Fig. 11 (b) show that the baseline model has no anomalies. In Fig. 11 (c) and Fig. 11 (d), the bolt damaged case indicates the anomalies are located mainly on the bottom right side of the plate, which is caused by the loosened bolt at the bottom fixture (a boundary condition change). The peak values are at least 10 times larger compared to the baseline model. However, there are other noticeable peaks at sensor 9 and sensor 24, especially in Fig. 11 (d). Such unrelated anomalies are usually caused by factors such as data acquisition errors, sensor calibration, and sensors malfunctions (e.g., sensors not fully attached to the plate). One of the common characteristics is those factors is the fact that they not related to the plate mechanics. Hence, we further improved the network by strengthening the interrelations between sensors and thus alleviating the environmental effects.

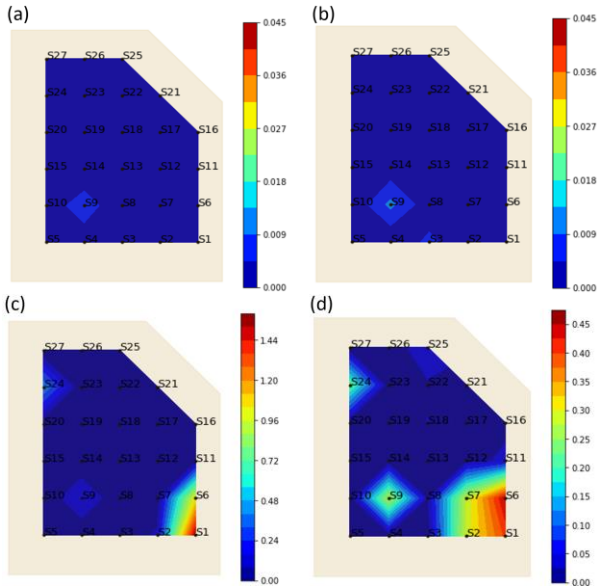


**FIGURE 11:** Modified error contours (a) parameter  $\mu$  results for undamaged plate; (b) parameter  $\sigma$  results for undamaged plate; (c) parameter  $\mu$  results for bolt loosening plate; (d) parameter  $\sigma$  results for bolt loosening plate.

### 4.3 Mechanics-based loss function and model retrain

From basic mechanics, strain changes at one location of the plate will result in strain changes around that location (influence area), which depends on the boundary condition, geometry, and loading conditions. To allow the network to learn such features from the baseline model, a mechanics inspired relations between the different sensor locations was incorporated with the loss function. Any abnormal datasets tested with the newly trained network would improve the classification accuracy of the anomalies if the data does not follow the learned baseline mechanical relations. The loss function is modified and an extra loss term  $loss_{spatial}$  was added to the original MSE loss function.  $loss_{spatial}$  and the modified loss function are defined below.

$$\Delta = y - x \quad (7)$$

$$loss_{spatial} = \frac{1}{N^2} \sum W_{ij} |\Delta_i - \Delta_j| \quad (8)$$

$$Modified\ loss = loss + loss_{spatial} \quad (9)$$

where  $x, y, \Delta$  and  $W$  refer to the input vector, the output vector, the difference between the input and output vectors and the spatial weight matrix, respectively.  $N$  denotes the number of the sensors under examination.

The weight matrix can be defined as:

$$W_{ij} = \varepsilon_i / \varepsilon_j \quad (10)$$

where  $\varepsilon_i$  refer to the strain at sensor  $i$ .

In Fig. 12, the modified losses vs epoch curves of the training and validation datasets are shown below. The absolute values are higher than the previous training results in Fig 6 because of the added spatial loss item.

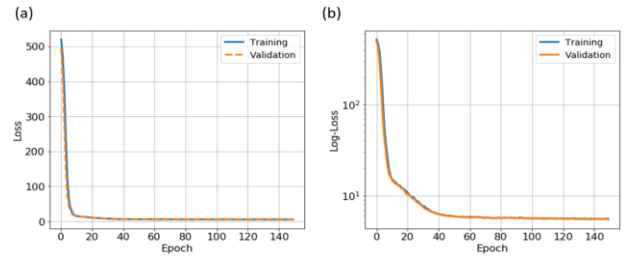


**FIGURE 12:** Modified training and validation losses with two scales (a) linear scale; (b) logarithmic scale.

### 4.4 Damage localization results

The AUROC contours from the training, validation, and testing dataset are shown in Fig. 13. Compared to Fig. 11 (a) and Fig. 11 (b), Fig. 13 (a) and Fig. 13 (b) also have contours values observed to be  $\cong 0.5$ , which means that there were no anomalies in the plate and the new baseline model is not affected by the modified network. In Fig. 13 (c) and Fig. 13 (d), the AUROC contours can obviously detect the anomalies, but the possible anomaly locations are not accurate. Noise in sensor 24 in Fig. 13 (c) and sensor 19 in Fig. 13 (d) reduce the accuracy. The red areas in the bottom right side in Fig. 13 (c) are covering too many sensors, which reduces the ability to localize the anomalies.

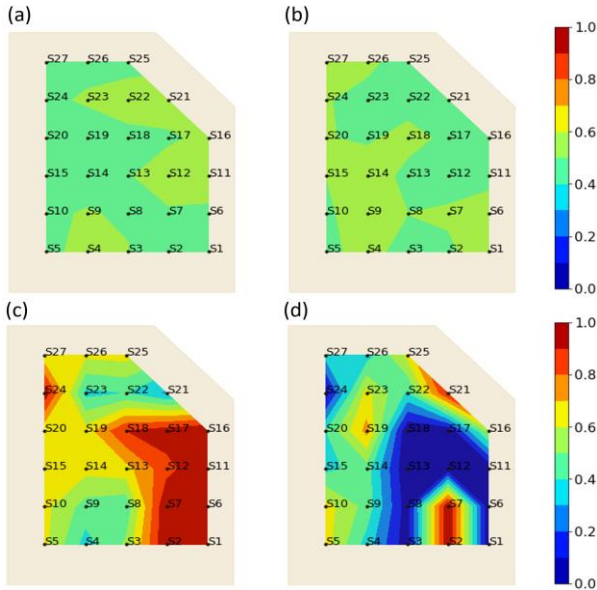


**FIGURE 13:** ROC contours using mechanics-based loss function (a) parameter  $\mu$  for undamaged plate; (b) parameter  $\sigma$  for undamaged plate; (c) parameter  $\mu$  for bolt damaged plate; (d) parameter  $\sigma$  for bolt damaged plate.

Fig. 14 shows the modified error contours from the mechanics-based anomaly detection network. Fig. 14 (a) and Fig. 14 (b) show similar results of the baseline model compared to Fig. 11 (a) and Fig. 11 (b), which use the MSE loss function for the network training. For Fig. 14 (c) and Fig. 14 (d), the modified network has improved its ability to enhance the peak values at the actual anomalies area (i.e., located at the bottom right corner of the plate), as the values are increased from 1.44 to 2.1 and 0.45 to 1.8, compared to Fig. 11 (c) and Fig. 11 (d) respectively. Also, the network eliminates undesired peak areas, and only the bottom right corner shows the anomaly contour, which is exactly where the bolt connection is located (i.e., between sensor 1 and sensor 2).

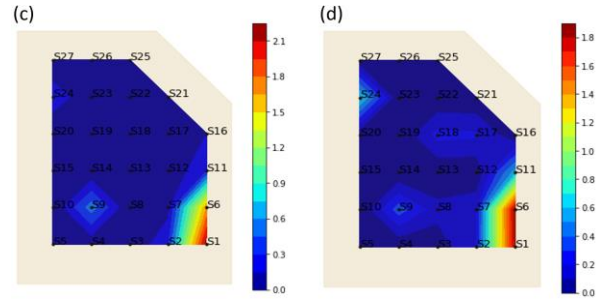
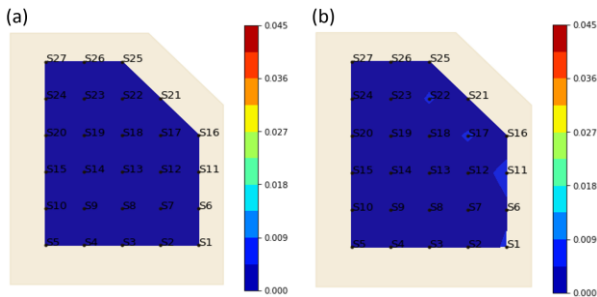


**FIGURE 14:** Modified error contours using mechanics-based loss function (a) parameter  $\mu$  for undamaged plate; (b) parameter  $\sigma$  for undamaged plate; (c) parameter  $\mu$  for bolt damaged plate (d) parameter  $\sigma$  for bolt damaged plate.

## 5. CONCLUSION

In this study, we proposed a mechanics-based deep anomaly detection neural network using compressed sensor data that can be applied to any structural component. The structure response data were measured at different locations of the component and then compressed based on probability distributions representation scheme. The compressed data were used for unsupervised network training by minimizing the reconstruction errors between the network input and output. After training, the output training and testing datasets were compared with different statistical methods such as loss histograms, ROC curves, and AUROC contours to classify the anomalies. A modified reconstruction error was defined to accurately localize the anomalies. We also presented a novel mechanics-based loss function. The retrained network established a relation between different sensors which enhances the performance of filtering out anomalies and finding the correct anomaly location. A gusset plate was tested and we successfully detected and localized the changed boundary condition at the bolt connections.

## ACKNOWLEDGEMENTS

This study was partially supported by the National Science Foundation Award CNS 1645783.

## REFERENCES

- [1] Zhang, L., G. Qiu, and Z.J.M. Chen, *Structural health monitoring methods of cables in cable-stayed bridge: A review*. 2021. **168**: p. 108343.
- [2] Sun, L., et al., *Review of bridge structural health monitoring aided by big data and artificial intelligence: From condition assessment to damage detection*. 2020. **146**(5): p. 04020073.
- [3] Li, Q., et al., *Structural health monitoring for a 600 m high skyscraper*. 2018. **27**(12): p. e1490.
- [4] Zhao, Y. *Structural Health Monitoring Applications in Tall Buildings*. in *E3S Web of Conferences*. 2020. EDP Sciences.
- [5] Hubbard, P.G., et al., *Dynamic structural health monitoring of a model wind turbine tower using distributed acoustic sensing (DAS)*. 2021. **11**(3): p. 833-849.

- [6] Civera, M. and C.J.S. Surace, *Non-Destructive Techniques for the Condition and Structural Health Monitoring of Wind Turbines: A Literature Review of the Last 20 Years*. 2022. **22**(4): p. 1627.
- [7] Ibrahim, A., et al., *A machine learning approach for structural health monitoring using noisy data sets*. 2019. **17**(2): p. 900-908.
- [8] Goyal, D. and B.J.A.o.C.M.i.E. Pabla, *The vibration monitoring methods and signal processing techniques for structural health monitoring: a review*. 2016. **23**(4): p. 585-594.
- [9] Wu, R.-T. and M.R.J.S.H.M. Jahanshahi, *Data fusion approaches for structural health monitoring and system identification: past, present, and future*. 2020. **19**(2): p. 552-586.
- [10] Azimi, M., G.J.C.A.C. Pekcan, and I. Engineering, *Structural health monitoring using extremely compressed data through deep learning*. 2020. **35**(6): p. 597-614.
- [11] Rocchetta, R., et al., *On-line Bayesian model updating for structural health monitoring*. 2018. **103**: p. 174-195.
- [12] Ye, X., T. Jin, and C.J.S.S.S. Yun, *A review on deep learning-based structural health monitoring of civil infrastructures*. 2019. **24**(5): p. 567-585.
- [13] Dong, C.-Z. and F.N.J.S.H.M. Catbas, *A review of computer vision-based structural health monitoring at local and global levels*. 2021. **20**(2): p. 692-743.
- [14] Azimi, M., A.D. Eslamlou, and G.J.S. Pekcan, *Data-driven structural health monitoring and damage detection through deep learning: State-of-the-art review*. 2020. **20**(10): p. 2778.
- [15] Fan, G., J. Li, and H.J.M. Hao, *Vibration signal denoising for structural health monitoring by residual convolutional neural networks*. 2020. **157**: p. 107651.
- [16] Abdeljaber, O., et al., *Real-time vibration-based structural damage detection using one-dimensional convolutional neural networks*. 2017. **388**: p. 154-170.
- [17] Khodabandehlou, H., et al., *Vibration-based structural condition assessment using convolution neural networks*. 2019. **26**(2): p. e2308.
- [18] Avci, O., et al., *Structural damage detection in real time: implementation of 1D convolutional neural networks for SHM applications*, in *Structural Health Monitoring & Damage Detection, Volume 7*. 2017, Springer. p. 49-54.
- [19] Choe, D.-E., H.-C. Kim, and M.-H.J.R.E. Kim, *Sequence-based modeling of deep learning with LSTM and GRU networks for structural damage detection of floating offshore wind turbine blades*. 2021. **174**: p. 218-235.
- [20] Zeng, Y., et al., *An innovative method for axial pressure evaluation in smart rubber bearing based on bidirectional long-short term memory neural network*. 2021. **182**: p. 109653.
- [21] Bao, X., Z. Wang, and G.J.O.E. Iglesias, *Damage detection for offshore structures using long and short-term memory networks and random decrement technique*. 2021. **235**: p. 109388.
- [22] Liu, G., et al., *Sensor faults classification for SHM systems using deep learning-based method with Tsfresh features*. 2020. **29**(7): p. 075005.
- [23] Li, L., et al., *FS-LSTM-Based Sensor Fault and Structural Damage Isolation in SHM*. 2020. **21**(3): p. 3250-3259.
- [24] Wang, Z. and Y.-J.J.S.H.M. Cha, *Unsupervised deep learning approach using a deep auto-encoder with a one-class support vector machine to detect damage*. 2021. **20**(1): p. 406-425.
- [25] Chow, J.K., et al., *Anomaly detection of defects on concrete structures with the convolutional autoencoder*. 2020. **45**: p. 101105.
- [26] Jayawardhana, M., et al., *Compressive sensing for efficient health monitoring and effective damage detection of structures*. 2017. **84**: p. 414-430.
- [27] Zhu, P., et al., *Zero shot detection*. 2019. **30**(4): p. 998-1010.
- [28] Wang, W., et al., *A survey of zero-shot learning: Settings, methods, and applications*. 2019. **10**(2): p. 1-37.
- [29] Rivera, A.R., et al., *Anomaly detection based on zero-shot outlier synthesis and hierarchical feature distillation*. 2020.
- [30] Sung, F., et al. *Learning to compare: Relation network for few-shot learning*. in *Proceedings of the IEEE conference on computer vision and pattern recognition*. 2018.
- [31] Xian, Y., et al., *Zero-shot learning—a comprehensive evaluation of the good, the bad and the ugly*. 2018. **41**(9): p. 2251-2265.
- [32] Lampert, C.H., et al., *Attribute-based classification for zero-shot visual object categorization*. 2013. **36**(3): p. 453-465.
- [33] Sony, S., et al., *A literature review of next-generation smart sensing technology in structural health monitoring*. 2019. **26**(3): p. e2321.
- [34] Qureshi, Y., et al., *Development of microscale flexible nylon/Ag strain sensor wire for real-time monitoring and damage detection in composite structures subjected to three-point bend test*. 2019. **181**: p. 107693.
- [35] dos Santos, F.L.M., et al. *The use of strain gauges in vibration-based damage detection*. in *Journal of Physics: conference series*. 2015. IOP Publishing.
- [36] Qureshi, Y., et al., *Real-time strain monitoring and damage detection of composites in different directions of the applied load using a microscale flexible Nylon/Ag strain sensor*. 2020. **19**(3): p. 885-901.
- [37] Zymelka, D., et al., *Printed strain sensor array for application to structural health monitoring*. 2017. **26**(10): p. 105040.
- [38] Yin, F., et al., *Stretchable, highly durable ternary nanocomposite strain sensor for structural health monitoring of flexible aircraft*. 2017. **17**(11): p. 2677.
- [39] Cui, H., et al., *Damage identification in a plate structure based on a cross-direction strain measurement method*. 2020. **158**: p. 107714.
- [40] Azim, M.R., M.J.S. Gül, and I. Engineering, *Data-driven damage identification technique for steel truss railroad bridges utilizing principal component analysis of strain response*. 2021. **17**(8): p. 1019-1035.
- [41] Wu, B., et al., *Damage identification method for continuous girder bridges based on spatially-distributed long-gauge strain sensing under moving loads*. 2018. **104**: p. 415-435.

- [42] Masri, S.F., et al., *Experimental study of embedded fiber-optic strain gauges in concrete structures*. 1994. **120**(8): p. 1696-1717.
- [43] Zhou, K. and Z.J.E.S. Wu, *Strain gauge placement optimization for structural performance assessment*. 2017. **141**: p. 184-197.
- [44] Chen, S.-Z., et al., *Damage detection of highway bridges based on long-gauge strain response under stochastic traffic flow*. 2019. **127**: p. 551-572.
- [45] ur Rehman, M.H., et al., *Big data reduction methods: a survey*. 2016. **1**(4): p. 265-284.
- [46] Ni, F., et al., *Deep learning for data anomaly detection and data compression of a long-span suspension bridge*. 2020. **35**(7): p. 685-700.
- [47] He, B. and Y.J.J.o.A.M. Li, *Big data reduction and optimization in sensor monitoring network*. 2014. **2014**.
- [48] Wu, M., L. Tan, and N.J.I.S. Xiong, *Data prediction, compression, and recovery in clustered wireless sensor networks for environmental monitoring applications*. 2016. **329**: p. 800-818.
- [49] Hasni, H., et al., *A new approach for damage detection in asphalt concrete pavements using battery-free wireless sensors with non-constant injection rates*. 2017. **110**: p. 217-229.
- [50] Hasni, H., et al. *Damage progression identification in asphalt concrete pavements: A smart self-powered sensing approach*. in *Advances in Materials and Pavement Prediction: Papers from the International Conference on Advances in Materials and Pavement Performance Prediction (AM3P 2018), April 16-18, 2018, Doha, Qatar*. 2018. CRC Press.
- [51] Hasni, H., et al., *Damage localization and quantification in gusset plates: A battery-free sensing approach*. 2018. **25**(6): p. e2158.
- [52] Li, T., et al. *Deep Unsupervised Anomaly Detection*. in *Proceedings of the IEEE/CVF Winter Conference on Applications of Computer Vision*. 2021.
- [53] Chalapathy, R. and S.J.a.p.a. Chawla, *Deep learning for anomaly detection: A survey*. 2019.
- [54] Chandola, V., A. Banerjee, and V.J.A.c.s. Kumar, *Anomaly detection: A survey*. 2009. **41**(3): p. 1-58.
- [55] Bereziński, P., B. Jasiul, and M.J.E. Szyrka, *An entropy-based network anomaly detection method*. 2015. **17**(4): p. 2367-2408.
- [56] An, N., et al. *Behavioral anomaly detection of malware on home routers*. in *2017 12th International Conference on Malicious and Unwanted Software (MALWARE)*. 2017. IEEE.
- [57] Pourhabibi, T., et al., *Fraud detection: A systematic literature review of graph-based anomaly detection approaches*. 2020. **133**: p. 113303.
- [58] Ahmed, M., A.N. Mahmood, and M.R.J.F.G.C.S. Islam, *A survey of anomaly detection techniques in financial domain*. 2016. **55**: p. 278-288.
- [59] Tang, Z., et al., *Convolutional neural network-based data anomaly detection method using multiple information for structural health monitoring*. 2019. **26**(1): p. e2296.
- [60] Bao, Y., et al., *Computer vision and deep learning-based data anomaly detection method for structural health monitoring*. 2019. **18**(2): p. 401-421.
- [61] Xu, D., et al. *An improved data anomaly detection method based on isolation forest*. in *2017 10th international symposium on computational intelligence and design (ISCID)*. 2017. IEEE.
- [62] Du, B., L.J.I.T.o.G. Zhang, and R. Sensing, *A discriminative metric learning based anomaly detection method*. 2014. **52**(11): p. 6844-6857.
- [63] Mao, J., H. Wang, and B.F.J.S.H.M. Spencer Jr, *Toward data anomaly detection for automated structural health monitoring: Exploiting generative adversarial nets and autoencoders*. 2021. **20**(4): p. 1609-1626.
- [64] Jeong, S., M. Ferguson, and K.H. Law. *Sensor data reconstruction and anomaly detection using bidirectional recurrent neural network*. in *Sensors and Smart Structures Technologies for Civil, Mechanical, and Aerospace Systems 2019*. 2019. SPIE.
- [65] Xu, X., et al., *Anomaly detection for large span bridges during operational phase using structural health monitoring data*. 2020. **29**(4): p. 045029.
- [66] Yuan, Z., et al., *An unsupervised method based on convolutional variational auto-encoder and anomaly detection algorithms for light rail squat localization*. 2021. **313**: p. 125563.
- [67] Shu, X., et al., *Unsupervised dam anomaly detection with spatial-temporal variational autoencoder*. 2022: p. 14759217211073301.
- [68] Bolandi, H., et al., *A novel data reduction approach for structural health monitoring systems*. 2019. **19**(22): p. 4823.